RSC Advances

PAPER

View Article Online
View Journal | View Issue

Open Access Article. Published on 10 February 2017. Downloaded on 11/26/2024 4:23:45 AM.
This article is licensed under a Creative Commons Attribution-NonCommercial 3.0 Unported Licence.

Cite this: *RSC Adv.*, 2017, **7**, 10891

Enhancement of As(v) adsorption from aqueous solution by a magnetic chitosan/biochar composite

Shaobo Liu,[ab] Binyan Huang,*[cd] Liyuan Chai,[a] Yunguo Liu,[cd] Guangming Zeng,[cd] Xin Wang,[e] Wei Zeng,[cd] Meirong Shang,[cd] Jiaqin Deng[cd] and Zan Zhou[cd]

Received 25th November 2016
Accepted 6th February 2017

DOI: 10.1039/c6ra27341f

rsc.li/rsc-advances

In this study, a magnetic chitosan/biochar composite (MCB) was prepared successfully, and characterized by SEM, TEM, VSM, XRD, FTIR, XPS, and zeta-potential to obtain its physical and chemical properties. The influence of different sorption parameters such as pH, contact time, initial As(v) concentration, and temperature on As(v) removal were studied thoroughly in order to optimize the reaction conditions. The results showed that the MCB adsorbed more As(v) (11.961 mg g^{-1}) than pristine biochar (3.681 mg g^{-1}). In addition, the adsorption behavior could be well described by a pseudo-second-order and Langmuir model. Thermodynamic parameters revealed that the sorption reaction was a spontaneous and endothermic process. The adsorbed MCB could be effectively regenerated by 1.0 mol L^{-1} NaOH, and the adsorption capacity decreased from 11.823 to 8.078 mg g^{-1} in five cycles. In conclusion, MCB could be used as an efficient adsorbent for environment purification and conveniently separated from aqueous solution after adsorption.

1. Introduction

Arsenic (As) is known as one of the most toxic chemical elements at very low concentrations, contamination of natural waters by inorganic arsenic (As) has dire consequences for public health all around the world because of its potential synonymy with toxicity.[1,2] The release of As can occur naturally from geothermal and groundwater,[3] or by anthropogenic activities, such as mining,[4] feed additives[5] and wood preservation.[6] High As concentrations in groundwater have been found in Argentina, Bangladesh, Chile, China, Hungary, Mexico, West Bengal (India), and Vietnam.[7,8] Ingestion of arsenic contaminated drinking water can result in both skin cancer and internal cancers, particularly of the lung and urinary tract.[9] The predominant form of inorganic arsenic commonly found in natural waters were oxyanions of trivalent arsenite (AsO_3^{3-}, As(III)) and pentavalent arsenate (AsO_4^{3-}, As(v)).[10] Although, As(v) tends to be less toxic compared with As(III), it is thermodynamically more stable due to which it predominates under normal conditions. Therefore, removal of As(v) is potentially important as As(III) irrespective of toxicity,[11] and removing As effectively from water supplies is essential to protecting environmental and human health.

Several methods have been developed to remove arsenic from water, such as, membrane technologies,[12] ion exchange,[13] oxidation/reduction,[14] oxidation–coagulation[15] and adsorption.[16] Among these techniques, the adsorption process is considered one of most promising techniques because it is economical, effective, and no sludge disposal. Various types of sorbents have been developed and applied for water treatment during the past few decades.[17]

Compared with conventional carbonaceous materials such as commercial activated carbon, the primary advantages of biochar are its low cost and a wealth of sources of biomass.[18,19] However, pristine biochar prepared from biomass feedstock without any treatment have relatively low heavy metal sorption capacity, and their sorption for aqueous As, which is in anionic forms of either arsenate (As(v)) or arsenite (As(III)), is relatively low due to most of biochar are predominantly net negatively charged on the surface.[20] Several methods have thus been developed to modify biochar to enhance its sorption for As. Chitosan is another sorbent that has been widely used to remove water pollutants because it is abundant, renewable, biodegradable and non-toxic in nature.[21] It is characterized by both large sorption capacity owing to the position of –OH and $–NH_2$ groups and high hydrophilicity with a large number of hydroxyl groups of glucose units and the presence of a large number of functional groups (acetamido, primary amino and/or hydroxyl groups).[22,23] Using chitosan modified biochar could

[a]School of Metallurgy and Environment, Central South University, Changsha 410083, P. R. China
[b]School of Architecture and Art, Central South University, Changsha 410083, P. R. China
[c]College of Environmental Science and Engineering, Hunan University, Changsha 410082, P. R. China. E-mail: hby617125216@163.com; Fax: +86 731 88822829; Tel: + 86 731 88649208
[d]Key Laboratory of Environmental Biology and Pollution Control, Hunan University, Ministry of Education, Changsha 410082, P. R. China
[e]College of Resources and Environmental Science, Hunan Normal University, Changsha 410006, P. R. China

Open Access Article. Published on 10 February 2017. Downloaded on 11/26/2024 4:23:45 AM.
This article is licensed under a Creative Commons Attribution-NonCommercial 3.0 Unported Licence.

show good performance to improve the adsorption ability of As(v).

Although the chitosan/biochar composite exhibited good sorption ability, it is cannot be separated easily from aqueous solution. Magnetic fluids have the capability to treat large number of wastewater within a short time and can be conveniently separated from wastewater. What's more, the magnetic fluids can increase the number of adsorption sites and enhance the adsorption capacity for arsenic.[24] Thus, coating chitosan with magnetic fluids can expand function of the chitosan, and the method has been reported that it can improve the surface area for adsorption.[25] Therefore, the magnetic chitosan modified with biochar could not only enhance the sorption ability but also be magnetically collected after adsorption.

The objective of this paper focused on enhancing the As(v) removal ability by the magnetic chitosan/biochar composite (MCB). The samples were characterized by Fourier transform infrared (FTIR), scanning electron microscope (SEM), transmission electron microscopy (TEM), vibrating sample magnetometry (VSM), X-ray photoelectron spectroscopy (XPS), X-ray diffraction (XRD) and zeta potential. In addition, kinetic, isothermal and thermodynamic analysis have been conducted in this paper. The desorption/regeneration properties of MCB were investigated to determine the reusability of adsorbent and evaluate the economic feasibility. The As(v) removal mechanisms was investigated by XPS analysis.

2. Materials and methods

2.1 Materials

All chemicals used in this study were purchased at analytical reagent grade and without any further purification. Rice straw (RS), the source of biomass, was obtained from Zhuzhou, Hunan province, China. Chitosan (95% acetylation degree) was provided by Hefei Bomei Biotechnology Co., Ltd. Glutaraldehyde was supplied by Sonopharm Chemical Reagent Co., Ltd. The disodium hydrogen arsenate heptahydrate ($Na_2HAsO_4 \cdot 7H_2O$) was purchased from Sigma Aldrich with a purity higher than 98%. The stock solution of 100 mg L^{-1} As(v) was prepared by dissolving 0.4165 g $Na_2HAsO_4 \cdot 7H_2O$ in 1 L ultra-water, and the required concentrations were obtained by diluting the stock solution with deionized water.

2.2 Preparation of adsorbent

The biomass was air-dried for two days, and subsequently oven-dried at 60 °C for 48 h. By pyrolysis of the biomass in a tube furnace at 450 °C with a heating rate of 5 °C min^{-1} under N_2 atmosphere for 2 h, the obtained biochar was ground and sieved through 150-mesh screen.

Magnetic fluid was prepared by co-precipitation method according to the former study.[26] Briefly, Fe^{2+} and Fe^{3+} (molar ratio 2 : 3) solution were added into the beaker with stirring at 55 °C and then dropwise NaOH solution with constant stirring for 10 min until pH reached 9.0. After adjusting the temperature of the reaction vessels to 65 °C, 0.8 mL Tween 80 was added into the mixture with stirring for another 30 min, and adjusted the pH value to 7.0. Then, the product was washed with Milli-Q water three times and was dispersed in ultrasonic device for 40 min. Finally, the solution was diluted to obtain magnetic fluid (40 g L^{-1}).

The magnetic chitosan modified with biochar (MCB) was synthesized as follow: 2.0 g chitosan was dissolved in 100 mL 2% acetic solution with stirring. Next, 10 mL magnetic fluid was added dropwise into the solution with constantly stirring for 30 min in a water bath at 50 °C. Then 1.0 g biochar was added with constantly stirring for another 60 min. After that, 4 mL glutaraldehyde was injected into the reaction system to form the gel and the pH of the reaction system was adjusted to 8.0–10.0. Finally, the mixture was kept in a water bath for a further 1 h. The precipitate were washed until the pH was about 7, and was dried at 60 °C, and sieved. The composite of chitosan modified with biochar (CB) was synthesized *via* the preparation of MCB without adding magnetic fluid.

2.3 Characterization and investigation of As(v) sorption by MCB

The morphologies of B and MCB were characterized by scanning electron microscopy (SEM) (JEOL JSM-6700. Japan) and transmission electron microscopy (TEM, Tecnai G2 F20, USA). The magnetization measurement of magnetic fluid and MCB were performed by vibrating sample magnetometer (VSM) (MPMS XL-7. America). The X-ray diffraction (XRD) patterns of CB and MCB were obtained by an X-ray diffractometer (Rigaku D/max-2500, Japan) with CuKα radiation. The Fourier transform infrared spectroscopy (FTIR) were measured on a spectrophotometer (Nicolet, Magna 550 spectrometer). Surface chemical composition of B, MCB were confirmed by an ESCALAB 250 Xi X-ray Photoelectron Spectrometer (XPS) (Thermo Fisher, USA). The iron ions concentrations were determined by a flame atomic absorption spectrometry (PerkinElmer AA700, USA). Zeta-potential of MCB was obtained from an Electroacoustic Spectrometer (ZEN3600 Zetasizer UK) under solution pH varying from 3.0 to 11.0.

2.4 Sorption experiments

All batch experiments were carried out with 20 mg adsorbent in a 50 mL conical flask with 20 mL As(v) aqueous solutions on a rotary shaker at 150 rpm for specific time. The pH of initial solutions was adjusted by HCl or NaOH. After being mixed for 24 h, the mixture was drawn and separated immediately by an aid of external magnet, and the residual concentrations was determined by atomic fluorescence spectroscopy (AFS-9700, China). The adsorption amount removed by the adsorbent, q_e (mg g^{-1}) was calculated as follows:

$$q_e = \frac{C_0 - C_e}{m} \times V \quad (1)$$

where C_0 (mg L^{-1}) and C_e (mg L^{-1}) are the initial and equilibrium concentration of As(v), V (L) is stand for the volume of solution, and m (g) is the weight of adsorbent.

The effect of pH on sorption experiment by three different materials (B, CB, MCB) were carried out by varying pH value

Open Access Article. Published on 10 February 2017. Downloaded on 11/26/2024 4:23:45 AM. This article is licensed under a Creative Commons Attribution-NonCommercial 3.0 Unported Licence.

between 3.0 and 11.0 with 15 mg L^{-1} As(v) for 24 h, and the mixtures were shaken with a speed of 150 rpm for 24 h at 25 °C.

The kinetic experiments were performed with different time intervals (0, 5, 15, 30, 60, 90, 120, 180, 240, 360, 480, 600, 1020, 1440 min) at pH 5.0, and the other parameters kept constant.

The isotherm experiments were conducted by varying initial concentrations from 0.2 mg L^{-1} to 50 mg L^{-1} at three different temperatures (25, 35, 45 °C), and adjusted pH value to 5.0.

All the experimental treatments were performed in three samples and the average values were reported. The relative errors of the data were generally within 5%.

2.5 Desorption experiment

The detailed desorption experiment was implemented as follows: the adsorbent which used to adsorb As(v) was added into 20 mL 1.0 mol L^{-1} NaOH solution with a shaking speed 150 rpm at 25 °C for 24 h. The adsorbent was subsequently washed to neutral and collected for recycling.

The resulted experimental data was obtained from the average of three measured value. The relative errors of the dada were within 5%.

3. Result and discussion

3.1 Characterization

3.1.1 SEM and TEM. The surface property is important for biochar reactivity and the magnification images of B and MCB are shown in Fig. 1. As shown in Fig. 1a, it could be obviously found that the surface of B was smooth and irregular. As can be seen in Fig. 1b, the prepared sample has a layered and porous structure due to the intrinsic nature of the biochar. It was noted in Fig. 1c that the MCB had an irregular surface with different shapes and many flakes, and the surface became much rougher and more heterogeneous, which might be attributed to the enhancement of superficial area. Compared with B in Fig. 1b, the surfaces of MCB in Fig. 1d had noticeable metal luster, indicating that the magnetic fluid had been assembled on the surface of MCB.

3.1.2 VSM. Fig. 2a show the VSM of magnetic fluid and MCB, and the typical hysteresis loop (S-like curve) were presented, which indicated super-magnetization of the composites.[27] The saturation magnetization is found to be 67.0 and 16.67 emu g^{-1} for magnetic fluid and MCB, respectively. This decline can be attributed to the relatively low amount of magnetic fluid, the existence of biochar and the surface modification by chitosan.[28] Although the saturation magnetization values of MCB are lower than that of bare magnetic fluid, the magnetic property of MCB remained high enough to meet the needs for magnetic separation. The inset in Fig. 2a demonstrated that MCB had a favorable separation characteristic and the feasibility of MCB for sequestrating As(v) from aqueous solution.

3.1.3 XRD. The XRD pattern of CB and MCB is illustrated in Fig. 2b. As can be seen, an amorphous structure was displayed in CB XRD pattern. However, there were six intense characteristic peaks in MCB at $2\theta = 30.1°$, 35.5°, 43.3°, 53.4°, 57.2° and 63.1°, which was corresponded to the primary diffraction of the (220), (311), (222), (400), (422) and (440) facets of the cubic spinel crystal planes of Fe_3O_4 (JCPDS card no. 16-0629).[29] The result indicated that magnetic fluid was coated with the composite successfully, and the final composite might be separated conveniently from aqueous solution by an external magnet field to avoid secondary pollution after As(v) adsorption.

3.1.4 FTIR. Fig. 2c shows the FTIR spectrum of B, CB and MCB. The stretching bands at about 1095 cm^{-1} (C–O), 1417 cm^{-1} ($-CH_2$), 1576 cm^{-1} (C=O) and 3371 cm^{-1} (–OH) were observed from RS biochar.[30] Similarly, in the FTIR spectra of CB, the same functional groups above mentioned were found around the corresponding wavenumber. However, the peak at

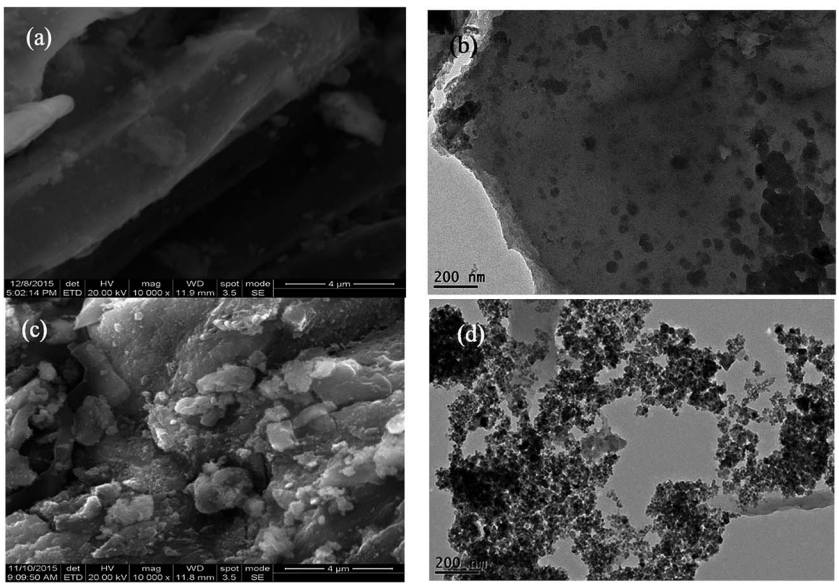

Fig. 1 The SEM images of (a) B, (c) MCB; the TEM images of (b) B, (d) MCB.

Open Access Article. Published on 10 February 2017. Downloaded on 11/26/2024 4:23:45 AM.
This article is licensed under a Creative Commons Attribution-NonCommercial 3.0 Unported Licence.

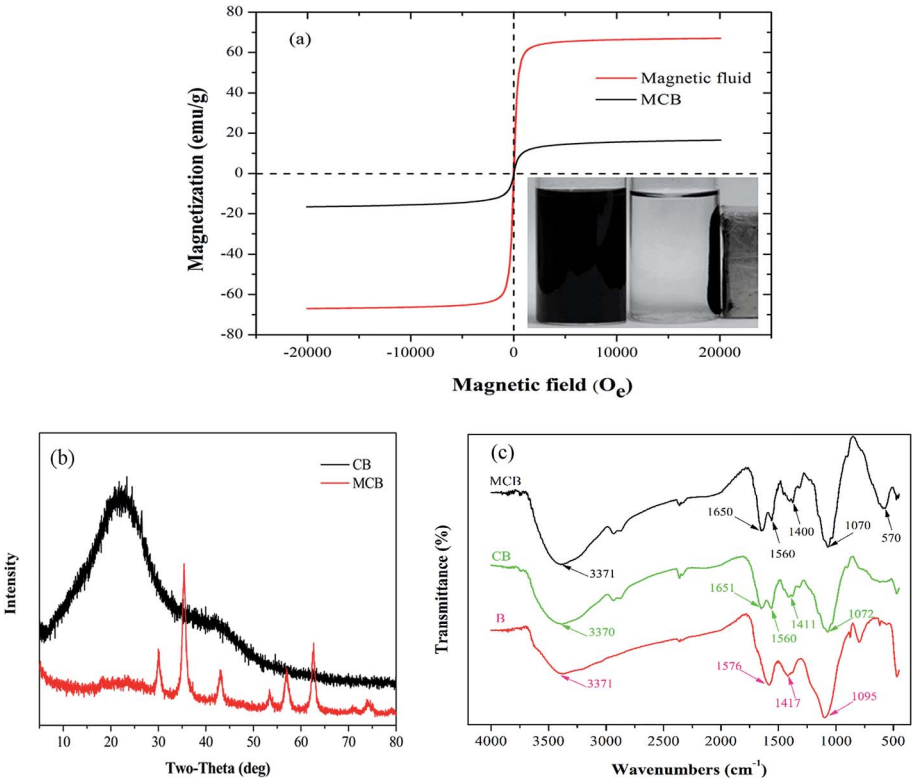

Fig. 2 (a) Magnetization curves of magnetic fluid and MCB at room temperature (the inset show the dispersion and magnetic separation of MCB). (b) XRD pattern of CB and MCB. (c) FTIR spectra of B, CB, and MCB.

1576 cm^{-1} shift to 1560 cm^{-1} ascribed to the amide I (C=O stretching) and a new peak was appeared at 1651 cm^{-1} ascribed to amide II (N–H blending modes), conforming that the carboxyl groups reacted with chitosan during the preparation of the composite.[31] In addition, it was obviously to find the stretching vibration of Fe–O peak appeared at around 570 cm^{-1} in MCB spectrum, and the results confirmed that the MCB was prepared successfully.

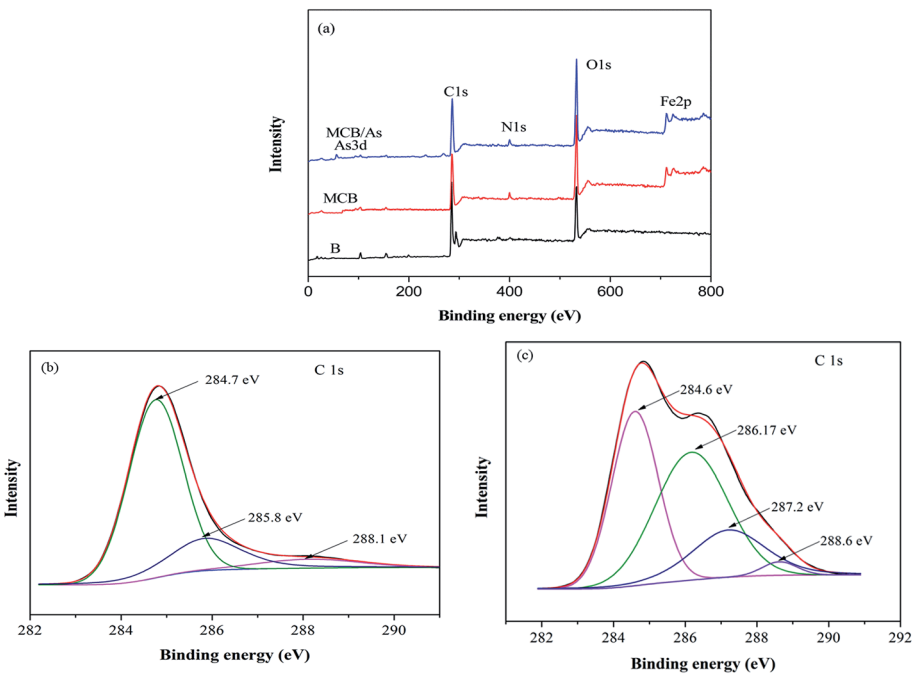

Fig. 3 (a) XPS wide-scan of B, MCB and MCB/As; C 1s XPS spectra of (b) B and (c) MCB.

Open Access Article. Published on 10 February 2017. Downloaded on 11/26/2024 4:23:45 AM.
This article is licensed under a Creative Commons Attribution-NonCommercial 3.0 Unported Licence.

3.1.5 XPS. To further understand the chemical ingredient of B and MCB, XPS was used to study the surface composition. The full scan XPS spectrum from 0 to 800 is displayed in Fig. 3a, and the photoelectron lines at about 284.7, 400.2 and 533.2 eV were corresponded to C 1s, N 1s and O 1s, respectively. Fig. 3b reflected the C 1s XPS spectra of B, three different peaks centered at 284.7, 285.8 and 288.1 eV were observed, which was attributed to the carbon atoms in the forms of C–C (72.1%), C–O (21.2%) and C=O (6.7%), respectively.[31] However, the C 1s XPS spectrum of MCB in Fig. 3c could be well curve-fitted into four peak components around 284.6, 286.17, 287.2, and 288.6 eV, which was corresponded to C–C (37.2%), C–O (42.7%), C–N (18.0%), and –COOH (2.1%), respectively. The difference between biochar and MCB was probably originated from modifying magnetic chitosan with pristine biochar, and the results further confirmed that MCB was prepared successfully, which were consistent with the FTIR characterization.

3.2 Effect of pH and comparison experiments

The pH value controls the interaction between adsorbate and adsorbents, which is predominant for the fractional species distribution of As(v) and the surface properties of adsorbents.[32] From Fig. 4a, the maximum adsorption capacity of B (3.681 mg g^{-1}), CB (10.600 mg g^{-1}), and MCB (11.533 mg g^{-1}) reached at pH 4.0, 3.0 and 5.0, respectively. For MCB, the sorption capacity increased slowly over the range of 3.0–5.0, and continually decreased from 5.0 to 10.0. This result can be interpreted as follows. In aqueous environment, there are two kind of arsenic species at pH range from 3.0 to 11.0, $H_2AsO_4^-$ is predominant when 3.0 < pH < 7.0, while $HAsO_4^{2-}$ is the main species at pH 7.0–11.0.[33] That is to say the main speciation of As(v) is anionic. As shown in Fig. 4b, the pH_{pzc} (point of zeta charge) of MCB was about 5.25. Under the condition pH < pH_{pzc}, the adsorbent was positively charged, which was beneficial for MCB combination with As(v). When pH > pH_{pzc}, the surface of MCB acquired negative charges, which could go against the As(v) adsorption due to electrostatic repulsion,[34] so as to the adsorption efficiency decreased significantly when the pH > 5.0. This result might confirm the hypothesis that electrostatic attraction could be one of the adsorption mechanisms. As it can be seen from Fig. 4a, As(v) adsorption onto three different materials was investigated at various pH. It was clearly to find that CB had an upper hand on As(v) adsorption compared with biochar, indicating that the introduction of chitosan was beneficial for removing As(v). It might be that $-NH_2$ and –OH from chitosan were protonated resulted in positively charged, which hold great promise for sequestrating As(v) due to electrostatic attraction. Thus, the sorption capacity of CB was much higher than biochar. Moreover, as shown in Fig. 4a, it can be also found that the sorption capacity of MCB was higher than that of CB, which is mainly due to the high surface areas and partial positive charges of magnetic fluid that have a strong affinity for As(v) in water.[35] However, the maximum adsorption of As(v) on MCB was appeared at pH 5, and the adsorption capacity was gradually reduced as the pH decreased, while the CB has the opposite trend, this is because of the easy oxidation/dissolution

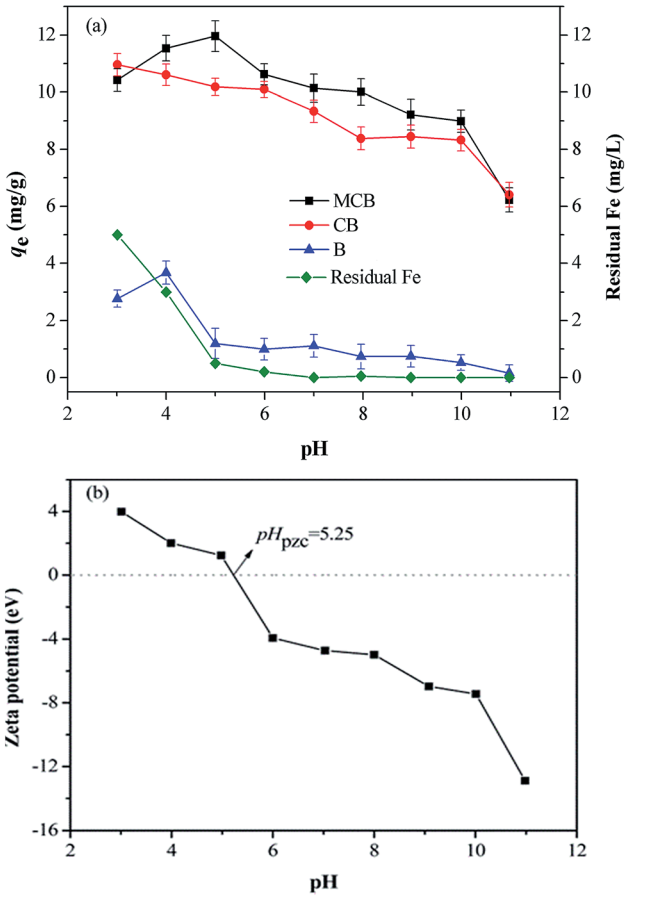

Fig. 4 (a) As(v) adsorption capacities of B, CB, MCB and residual Fe in solution with varying pH; (b) zeta-potential of MCB at different solution pH.

of iron nanoparticles, especially at high concentrations of acid solution that lead to a decrease in the sorption capacity of MCB. At the same time, we found that the stronger the acidity, the more dissolved iron ions were detected by the flame atomic absorption (Fig. 4a). When pH increases to 5 and above, leaching of Fe ion significantly reduces. The composite MCB is stable when the pH is above 5. All in all, MCB had superiority in As(v) removal, and could be conveniently separated from after adsorption aqueous solution compared with B and CB.

3.3 Effect of co-existing ions

Considering the complexity of water resources, the existence of various ions, such as Cl^-, NO_3^-, CO_3^{2-}, SO_4^{2-} and PO_4^{3-} ions might influence the uptake capacity of MCB to As(v). Therefore, the effect of co-existing ions on adsorption was conducted by batch experiments at different concentrations of NaCl, $NaNO_3$, Na_2CO_3, Na_2SO_4, and Na_3PO_4, and the obtained results are shown in Fig. 5. The adsorption capacity of MCB was decreased in the concentrations of various anions from 0 to 1.0 mol L^{-1}, which might be attributed to the competition between negatively charged anions and $HAsO_4^-$. These anions could be easily captured by the adjacent hydroxyl or carboxyl groups that were present on the surface of MCB, which might change the surface

Open Access Article. Published on 10 February 2017. Downloaded on 11/26/2024 4:23:45 AM.
This article is licensed under a Creative Commons Attribution-NonCommercial 3.0 Unported Licence.

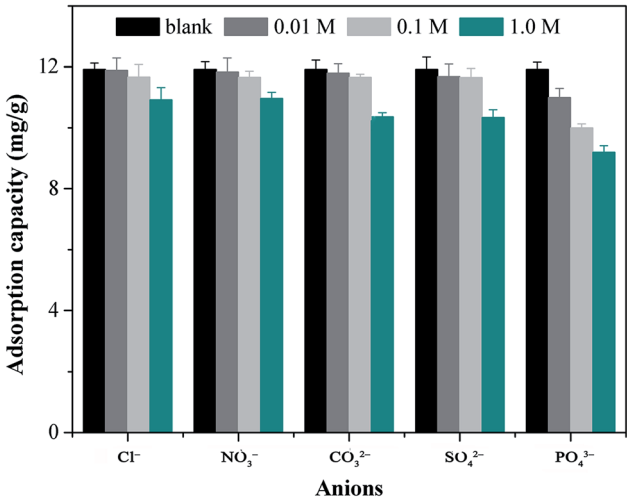

Fig. 5 Effect of various co-existing anions on As(v) adsorption for MCB.

state of MCB and decrease the availability of binding sites.[36] On the other hand, it was observed that the presence of CO_3^{2-} and SO_4^{2-} had a greater impact on As(v) removal compared with the Cl^- and NO_3^-, however, PO_4^{3-} could cause the greatest decrease in As(v) adsorption, which might be due to the strong competition between the PO_4^{3-} and As(v) for the binding sites of the adsorbent. Thus, it might occupy more adsorption sites compared to the other anions. In the practical application, some pretreatment before adsorption to reduce the concentration of various anions might be beneficial for contaminant removal.

3.4 Effect of contact time and adsorption kinetics

The effect of contact time on As(v) adsorption onto MCB is illustrated in Fig. 6a, and the inset shows the linear plot of pseudo-second-order. The adsorption process could be divided into two regions. In the first stage, the adsorption rate was very fast, and over 90% of the equilibrium adsorption capacity was achieved within 30 min, which could be owing to the existence of abundant active sites on the surface of adsorbents. In the subsequent step, the process was slow, and the equilibrium was reached in about 3 h. It might be attributed to the great decline of binding sites on adsorbents surface and the aggregation between particles.[37] The kinetic of As(v) adsorption onto MCB was applied in order to understand the adsorption behaviors of MCB composite. The adsorption data of As(v) at different time intervals was simulated by pseudo-first-order and pseudo-second-order model. The equations are illustrated as follows:

Non-linear pseudo-first-order:

$$q_t = q_{e,1}(1 - e^{-k_1 t}) \tag{2}$$

Non-linear pseudo-second-order:

$$q_t = \frac{q_{e,2}^2 k_2 t}{1 + q_{e,2} k_2 t} \tag{3}$$

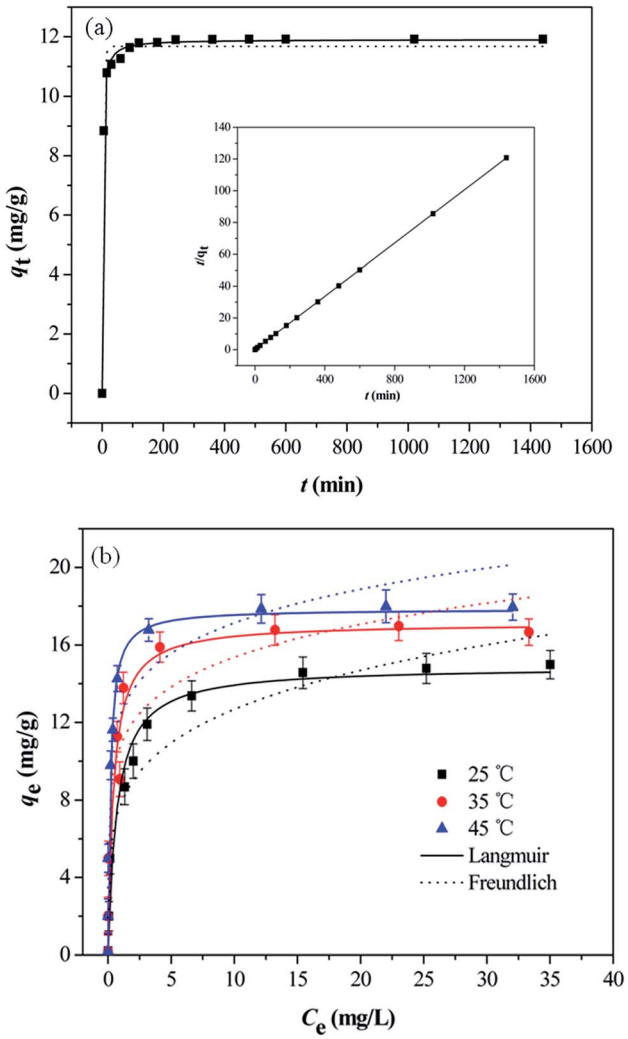

Fig. 6 (a) Pseudo-first-order (dot line) and pseudo-second-order (solid line) non-linear plots of adsorption kinetics for As(v) onto MCB. (b) Langmuir and Freundlich non-linear plots of isotherm for As(v) adsorption onto MCB at different temperatures.

Linear pseudo-second-order:

$$\frac{t}{q_t} = \frac{1}{k_2 q_{e,2}^2} + \frac{t}{q_e} \tag{4}$$

where q_t (mg g^{-1}) is the mass of As(v) adsorbed per gram at time t (min), $q_{e,1}$ and $q_{e,2}$ (mg g^{-1}) are the adsorption capacity calculated by pseudo-first-order and pseudo-second-order model, respectively, k_1 (min^{-1}) and k_2 (g mg^{-1} min^{-1}) are the adsorption rate constant of pseudo-first-order and pseudo-second-order model. After being fitted by these models, the calculated parameters are listed in Table 1. It was obviously to find that the correlation coefficient (R^2) of pseudo-second-order (0.999) was higher than the pseudo-first-order (0.988), and the calculated q_e represented a better agreement with the detected values in experiment. Therefore, the adsorption kinetics of As(v) onto MCB could be well-described by pseudo-second-order model, suggesting a chemisorption process might be involved in adsorption.

Open Access Article. Published on 10 February 2017. Downloaded on 11/26/2024 4:23:45 AM.
This article is licensed under a Creative Commons Attribution-NonCommercial 3.0 Unported Licence.

Table 1 Kinetic parameters for adsorption of As(v) onto MCB

Pseudo-first-order model			Pseudo-second-order model			
k_1 (min^{-1})	q_e (mg g^{-1})	R^2	k_2 (g mg^{-1} min^{-1})	q_e (mg g^{-1})	R^2	$q_{e,exp}$ (mg g^{-1})
0.273	11.681	0.988	0.048	11.907	0.999	11.920

3.5 Adsorption isotherm

To describe the equilibrium established between adsorbed As(v) on the adsorbent and the remaining As(v) in the solution, two widespread-used isotherm models (Langmuir and Freundlich models) were applied to describe the equilibrium characteristics of the adsorption. The Langmuir adsorption model assumed that all the binding sites were equal and the adsorbent surface is homogeneous, while the Freundlich isotherm model was an empirical equation for explaining heterogeneous adsorption process.[38] Both the two models were expressed as follows:

Langmuir:

$$q_e = \frac{q_{max} K_L C_e}{1 + K_L C_e} \tag{5}$$

Freundlich:

$$q_e = K_F C_e^{1/n} \tag{6}$$

where C_e and q_e (mg g^{-1}) represent the equilibrium concentration and the adsorption capacity at equilibrium, respectively, q_{max} (mg g^{-1}) is the maximum adsorption capacity, K_L (L mg^{-1}) is the constant that related to free energy of adsorption; K_F is the Freundlich constant related to sorption capacity; n is the empirical parameter varied with the degree of heterogeneity of adsorbing sites.

Fig. 6b showed As(v) sorption isotherms on the MCB at three different temperatures. The relative parameters calculated from the Langmuir and Freundlich isotherm models were listed in Table 2. As can be seen from Fig. 6b, the sorption isotherm maximum (17.876 mg g^{-1}) was at 45 °C and minimum (14.928 mg g^{-1}) at 25 °C. This result indicated that As(v) sorption on the MCB was promoted at higher temperature. According to the coefficient correlation (R^2) obtained from Table 2, Langmuir isotherm had a better fitting model than the Freundlich isotherms model, suggesting that As(v) sorption on the MCB was a monolayer coverage. Additionally, K_L increased with the increasing of the temperature, which indicated that the adsorption of As(v) onto MCB was an endothermic process. Another parameter R_L, a dimensionless constant separation parameter, is given by the following equation:

$$R_L = \frac{1}{1 + K_L C_0} \tag{7}$$

where C_0 is the highest initial concentration of As(v) (mg L^{-1}). This parameter indicates that the isotherm is unfavorable ($R_L > 1$), favorable ($0 < R_L < 1$), linear ($R_L = 1$), or irreversible ($R_L = 0$).[39] In this study, R_L values calculated between 0.003 and 0.015, which proves that the adsorption is a favorable process. In comparison with other adsorbents at different solution pH (Table 3), the maximum As(v) sorption capacity of MCB was greater than many previous reported adsorbents.[17,40–42]

3.6 Adsorption thermodynamic studies

Thermodynamic parameters such as the Gibbs free energy change (ΔG°), enthalpy change (ΔH°), and entropy change (ΔS°) were used to evaluate the feasibility and nature of adsorption reaction. They were determined by using the following equations:

$$\Delta G^\circ = -RT \ln K^\circ \tag{8}$$

$$\ln K^\circ = \frac{\Delta S^\circ}{R} - \frac{\Delta H^\circ}{RT} \tag{9}$$

where R (8.314 J mol^{-1} K^{-1}) is universal gas constant and T (K) is the solution temperature. K° is the adsorption equilibrium constant, which was calculated by plotting ln K_d ($K_d = q_e/C_e$) *versus* C_e and extrapolating C_e to zero.

Table 3 Comparison of the maximum As(v) adsorption capacity with other adsorbents

Adsorbents	Solution pH	Adsorption capacity (mg g^{-1})	References
Charred dolomite	7.2	2.157	40
Iron-impregnated biochar	5.8	2.160	17
Activated bauxite	3.5	6.900	41
Activated alumina	2.6	12.340	42
Magnetic chitosan biochar	5.0	17.876	This study

Table 2 Langmuir and Freundlich isotherm parameters for adsorption of As(v) onto MCB

	Langmuir			Freundlich		
Temperature (°C)	q_{max} (mg g^{-1})	K_L (L mg^{-1})	R^2	K_F (L mg^{-1})	n	R^2
25	14.928	1.354	0.970	7.839	4.703	0.914
35	17.164	2.275	0.906	10.604	6.094	0.898
45	17.876	5.805	0.945	11.992	6.676	0.900

Open Access Article. Published on 10 February 2017. Downloaded on 11/26/2024 4:23:45 AM.
This article is licensed under a Creative Commons Attribution-NonCommercial 3.0 Unported Licence.

Table 4 Thermodynamic parameters for As(v) onto MCB

ln K°			ΔG° (kJ mol^{-1})				
25 °C	35 °C	45 °C	25 °C	35 °C	45 °C	ΔH° (kJ mol^{-1})	ΔS° (kJ mol^{-1} K^{-1})
−0.985	1.410	1.544	−2.442	−3.612	−4.083	232.630	56.836

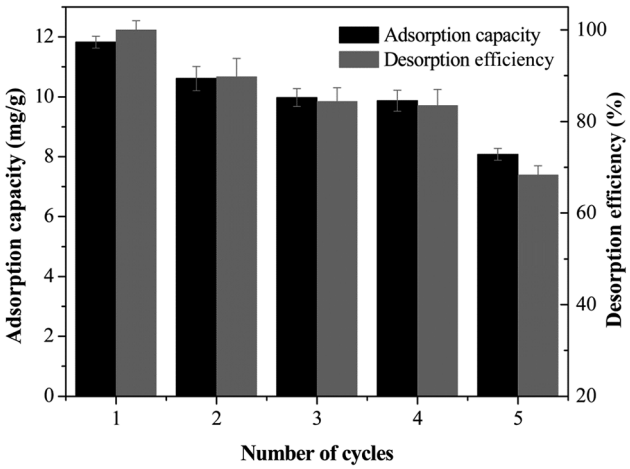

Fig. 7 Five consecutive adsorption–desorption cycles of MCB for As(v) removal.

Thermodynamic analysis was investigated at three different temperatures (25, 35, and 45 °C). The calculated results are shown in Table 4. The ΔH° and ΔS° values were found to be 232.630 kJ mol^{-1} and 56.836 J mol^{-1} K^{-1}, respectively. The ΔG° values were negative at the studied temperature, which was −2.442 kJ mol^{-1}, −3.612 kJ mol^{-1} and −4.083 kJ mol^{-1}, at 25, 35, and 45 °C, respectively. It was obvious that the ΔG° values became more negative as the temperature increased, which indicated that the adsorption was spontaneity and more favorable at high temperature. The positive ΔH° value implied that the adsorption reaction was endothermic, and it was the reason why the adsorption capacity of As(v) increased along with the increase of temperature. This was consistent with the isotherm analysis at different temperature. In addition, the positive ΔS° indicated that the degrees of freedom increased at the solid–liquid interface during the adsorption process.

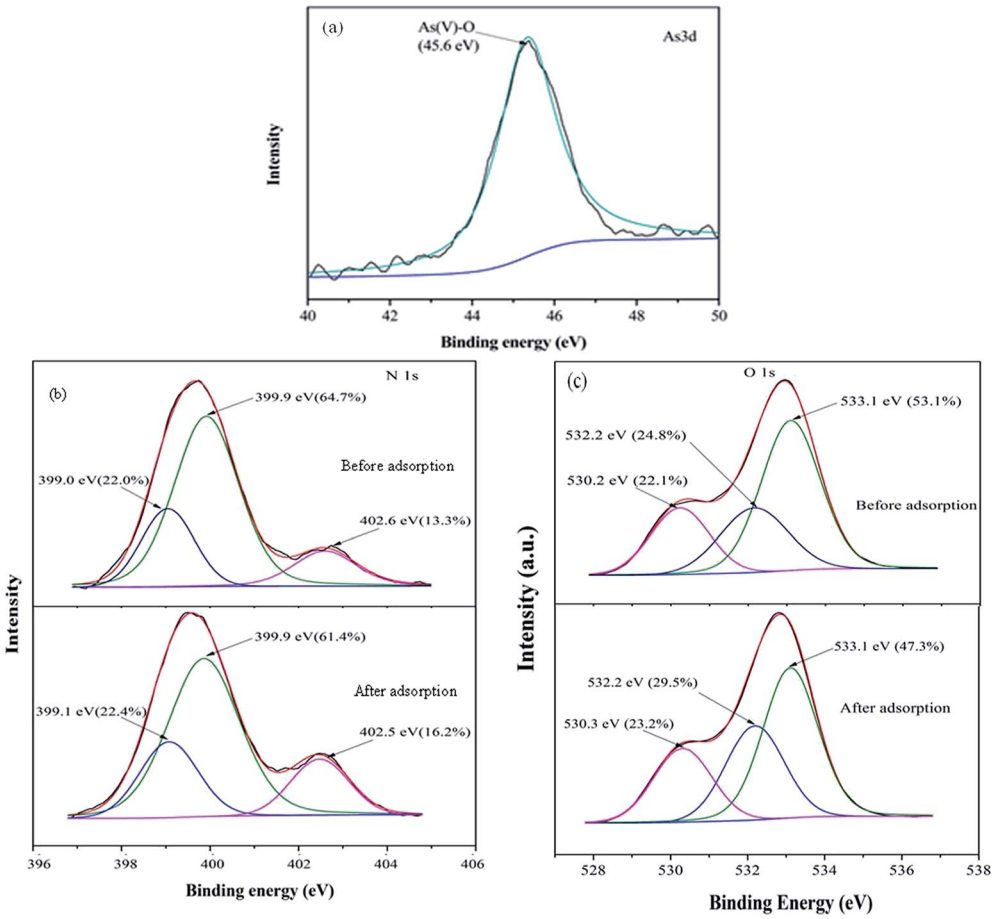

Fig. 8 The XPS high-resolution spectra of (a) As 3d, (b) N 1s and (c) O 1s.

Open Access Article. Published on 10 February 2017. Downloaded on 11/26/2024 4:23:45 AM.
This article is licensed under a Creative Commons Attribution-NonCommercial 3.0 Unported Licence.

3.7 Reusability of adsorbent

The reversibility and desorption efficiency are important parameters to determine the reusability and economic feasibility. In this study, 1.0 mol L^{-1} NaOH solution was selected as a stripping reagent to study the reusability and desorption efficiency for 5 times, and the results are presented in Fig. 7. The MCB maintained 11.823 mg g^{-1} adsorption capacity for As(v) after one adsorption–desorption cycle. After 5 cycles of reuse, the regenerated MCB still retained about 8.078 mg g^{-1} uptake capacity for As(v), indicting a good reusability of adsorbent for As(v) removal. However, the decreasing of adsorption capacity could be assigned to the reduction of surface area and pore volume, and the relatively weak functional groups.[34] The desorption efficiency was decreased slowly from 98% to 68%, and it still presented a relatively high removal efficiency after 5 adsorption–desorption experiments.

3.8 Adsorption mechanism

To investigate the mechanism of As(v) removal, XPS analysis has been carried out and the wide XPS spectra of the MCB composite after As(v) adsorption was given in Fig. 3a. After As(v) adsorption, typical As 3d XPS peak appeared. In Fig. 8a, which was assigned to the As(v)–O,[43] so it can be demonstrated MCB could be used to eliminate As(v) from aqueous solution. Furthermore, Fig. 8b reflected the N 1s XPS spectra of MCB before and after As(v) adsorption. The N 1s spectrum of MCB could be deconvoluted into three peak component with binding energies (BEs) at 399.0, 399.9, and 402.5 eV, which were consistent with the amine (–NH_2), amide(–NH–), and protonated amine (N^+), respectively.[44] After As(v) adsorption, the molar ratio of N^+ increased significantly from 13.3% to 16.2%, the –NH– decreased from 64.7% to 61.4%, and the –NH_2 had little changes, which indicated that the N^+ might play a key role in As(v) removal owing to the presence of N^+ could absorb negatively charged $H_2AsO_4^-$ or $HAsO_4^{2-}$ through electrostatic attraction and it was explained that the removal efficiency of As(v) was significantly improved after grafting chitosan on biochar. The O 1s XPS spectrum of MCB composite before and after adsorption is shown in Fig. 8c. It was noted that there were three peaks centered at 530.2, 532.2 and 533.1 eV in MCB spectra, which was assigned to Fe–O (22.1%), –OH (24.8%) and O–C–O (53.1%).[45] However, after As(v) adsorption, the molar ratio of the surface Fe–O groups increased to 23.2%, which might be due to the formation of Fe–O–As groups on the adsorbent surface after As(v) adsorption, and it also explains why the magnetic fluid modification greatly enhanced CB's sorption ability to As(v). Furthermore, the peaks at 532.2 eV due to –OH group, and the molar ratio increased from 24.8% to 29.5%, which might be owing to the reaction between –OH from MCB and As(v) *via* electrostatic attraction, and the results were consistent with the pH analysis.

4. Conclusion

The magnetic chitosan/biochar composite (MCB) was prepared successfully as a low-cost adsorbent to remove As(v) from aqueous solution. The adsorption experiment indicated that there was an obvious enhanced adsorption capacity of As(v) after modification. The experimental data was better fitted by the pseudo-second-order and Langmuir model, and the maximum adsorption capacity (17.876 mg g^{-1}) was obtained at pH 5, 45 °C. The sorption reaction was an endothermic and spontaneous process. Based on the experiments, the interaction between As(v) and MCB might include electrostatic attraction and the increased adsorption sites that iron provided.

Acknowledgements

This work was supported by the National Natural Science Foundation of China (Grant no. 51609268, 41271332, 51521006 and 51478470).

References

1 I. Andjelkovic, D. N. Tran, S. Kabiri, S. Azari, M. Markovic and D. Losic, *ACS Appl. Mater. Interfaces*, 2015, **7**, 9758–9766.
2 C. H. Liu, Y. H. Chuang, T. Y. Chen, Y. Tian, H. Li, M. K. Wang and W. Zhang, *Environ. Sci. Technol.*, 2015, **49**, 7726–7734.
3 C.-W. Huang, C.-C. Wei and V. H.-C. Liao, *Chemosphere*, 2015, **141**, 44–49.
4 Q. Sun, Y. Song, S. Liu, F. Wang, L. Zhang, S. Xi and G. Sun, *Atmos. Environ.*, 2015, **118**, 1–6.
5 X. Liu, W. Zhang, Y. Hu and H. Cheng, *Microchem. J.*, 2013, **108**, 38–45.
6 S. S. Nielsen, L. Petersen, P. Kjeldsen and R. Jakobsen, *Chemosphere*, 2011, **84**, 383–389.
7 H. Guo, D. Wen, Z. Liu, Y. Jia and Q. Guo, *Appl. Geochem.*, 2014, **41**, 196–217.
8 J. Tong, H. Guo and C. Wei, *Sci. Total Environ.*, 2014, **496**, 479–487.
9 H. Guo, Y. Ren, Q. Liu, K. Zhao and Y. Li, *Environ. Sci. Technol.*, 2013, **47**, 1009–1016.
10 P. Smedley and D. Kinniburgh, *Appl. Geochem.*, 2002, **17**, 517–568.
11 P. Chutia, S. Kato, T. Kojima and S. Satokawa, *J. Hazard. Mater.*, 2009, **162**, 440–447.
12 O. Coronell, B. Mi, B. J. Mariñas and D. G. Cahill, *Environ. Sci. Technol.*, 2012, **47**, 420–428.
13 A. Dominguez-Ramos, K. Chavan, V. n. García, G. Jimeno, J. Albo, K. V. Marathe, G. D. Yadav and A. Irabien, *Ind. Eng. Chem. Res.*, 2014, **53**, 18920–18927.
14 A. Molinari, L. Guadagnini, M. Marcaccio, S. Straface, X. Sanchez-Vila and A. Guadagnini, *Sci. Total Environ.*, 2013, **444**, 231–240.
15 S. Bordoloi, S. K. Nath, S. Gogoi and R. K. Dutta, *J. Hazard. Mater.*, 2013, **260**, 618–626.
16 I. Ali, *Chem. Rev.*, 2012, **112**, 5073–5091.
17 X. Hu, Z. Ding, A. R. Zimmerman, S. Wang and B. Gao, *Water Res.*, 2015, **68**, 206–226.
18 L. Lou, L. Yao, G. Cheng, L. Wang, Y. He and B. Hu, *PLoS One*, 2015, **10**, e0137467.

Open Access Article. Published on 10 February 2017. Downloaded on 11/26/2024 4:23:45 AM.
This article is licensed under a Creative Commons Attribution-NonCommercial 3.0 Unported Licence.

19 X. Tan, Y. Liu, G. Zeng, X. Wang, X. Hu, Y. Gu and Z. Yang, *Chemosphere*, 2015, **125**, 70–85.
20 L. Beesley and M. Marmiroli, *Environ. Pollut.*, 2011, **159**, 474–480.
21 Y. Zhou, B. Gao, A. R. Zimmerman, J. Fang, Y. Sun and X. Cao, *Chem. Eng. J.*, 2013, **231**, 512–518.
22 B. Huang, Y. Liu, B. Li, G. Zeng, X. Hu, B. Zheng, T. Li, L. Jiang, X. Tan and L. Zhou, *RSC Adv.*, 2015, **5**, 106339–106349.
23 A. Adamczuk and D. Kołodyńska, *Chem. Eng. J.*, 2015, **274**, 200–212.
24 Y.-F. Lin, J.-L. Chen, C.-Y. Xu and T.-W. Chung, *Chem. Eng. J.*, 2014, **250**, 409–415.
25 L. Fan, C. Luo, X. Li, F. Lu, H. Qiu and M. Sun, *J. Hazard. Mater.*, 2012, **215–216**, 272–279.
26 X. J. Hu, J. S. Wang, Y. G. Liu, X. Li, G. M. Zeng, Z. L. Bao, X. X. Zeng, A. W. Chen and F. Long, *J. Hazard. Mater.*, 2011, **185**, 306–314.
27 C. Cao, L. Xiao, C. Chen, X. Shi, Q. Cao and L. Gao, *Powder Technol.*, 2014, **260**, 90–97.
28 H. Deng, X. Li, Q. Peng, X. Wang, J. Chen and Y. Li, *Angew. Chem.*, 2005, **117**, 2842–2845.
29 F.-y. Guo, Y.-g. Liu, H. Wang, G.-m. Zeng, X.-j. Hu, B.-h. Zheng, T.-t. Li, X.-f. Tan, S.-f. Wang and M.-m. Zhang, *RSC Adv.*, 2015, **5**, 45384–45392.
30 B. Chen, Z. Chen and S. Lv, *Bioresour. Technol.*, 2011, **102**, 716–723.
31 M.-m. Zhang, Y.-g. Liu, T.-t. Li, W.-h. Xu, B.-h. Zheng, X.-f. Tan, H. Wang, Y.-m. Guo, F.-y. Guo and S.-f. Wang, *RSC Adv.*, 2015, **5**, 46955–46964.
32 K. Elwakeel, *Int. J. Environ. Sci. Technol.*, 2014, **11**, 1051–1062.
33 M. X. Loukidou, K. A. Matis, A. I. Zouboulis and M. Liakopoulou-Kyriakidou, *Water Res.*, 2003, **37**, 4544–4552.
34 C. Gan, Y. Liu, X. Tan, S. Wang, G. Zeng, B. Zheng, T. Li, Z. Jiang and W. Liu, *RSC Adv.*, 2015, **5**, 35107–35115.
35 Y.-F. Pan, C. T. Chiou and T.-F. Lin, *Environ. Sci. Pollut. Res.*, 2010, **17**, 1401–1410.
36 H. Wang, X. Yuan, Y. Wu, H. Huang, G. Zeng, Y. Liu, X. Wang, N. Lin and Y. Qi, *Appl. Surf. Sci.*, 2013, **279**, 432–440.
37 L. Fan, C. Luo, M. Sun, X. Li and H. Qiu, *Colloids Surf., B*, 2013, **103**, 523–529.
38 E. Agrafioti, D. Kalderis and E. Diamadopoulos, *J. Environ. Manage.*, 2014, **133**, 309–314.
39 Z. Wu, X. Yuan, H. Zhong, H. Wang, G. Zeng, X. Chen, H. Wang, L. Zhang and J. Shao, *Sci. Rep.*, 2016, **6**, 25638.
40 Y. Salameh, A. B. Albadarin, S. Allen, G. Walker and M. N. M. Ahmad, *Chem. Eng. J.*, 2015, **259**, 663–671.
41 H. S. Altundoğan, S. Altundoğan, F. Tümen and M. Bildik, *Waste Manag.*, 2002, **22**, 357–363.
42 T.-F. Lin and J.-K. Wu, *Water Res.*, 2001, **35**, 2049–2057.
43 Y.-X. Zhang and Y. Jia, *Appl. Surf. Sci.*, 2014, **290**, 102–106.
44 X. Yang, Y. Tu, L. Li, S. Shang and X.-m. Tao, *ACS Appl. Mater. Interfaces*, 2010, **2**, 1707–1713.
45 N. A. Travlou, G. Z. Kyzas, N. K. Lazaridis and E. A. Deliyanni, *Langmuir*, 2013, **29**, 1657–1668.

 This journal is © The Royal Society of Chemistry 2017